Enhancing the Detection Power of CUSUM Charts for Changes in the Mean of the Long-Memory ARFIMAX Model with Exponential White Noise

Yupaporn Areepong
Department of Applied Statistics, Faculty of Applied Science, King Mongkut's University of Technology North Bangkok, Thailand
yupaporn.a@sci.kmutnb.ac.th

Wilasinee Peerajit
Department of Applied Statistics, Faculty of Applied Science, King Mongkut's University of Technology North Bangkok, Thailand
wilasinee.p@sci.kmutnb.ac.th (corresponding author)

Received: 5 July 2025 | Revised: 27 July 2025, 22 August 2025, and 24 August 2025 | Accepted: 30 August 2025

 DOI: https://doi.org/10.48084/etasr.13174

ABSTRACT

The Cumulative Sum (CUSUM) control chart is highly effective in detecting small to moderate shifts in process means, making it a key tool for quality control. Its performance is commonly evaluated using the Average Run Length (ARL), defined as the expected number of samples before signaling an out-of-control condition. Traditional ARL estimation techniques, such as Monte Carlo simulations, Markov chains, and numerical Integral Equation (IE) methods, are computationally demanding and yield only approximate results. This paper presents a new explicit ARL computation method derived from the IE framework, with its validity established through Banach's fixed point theorem. The method is applied to the CUSUM chart for monitoring a long-memory ARFIMAX process with exponential white noise. Benchmark comparisons with accurate but costly numerical IE methods (Midpoint, Trapezoidal, and Simpson's Rules) indicate that the proposed method achieves near-perfect accuracy in a fraction of the time. Furthermore, a shift size of 0.75 provided the fastest detection, and a case study confirmed its effectiveness for real-time process monitoring.

Keywords-Cumulative Sum (CUSUM) control chart; Average Run Length (ARL); long-memory ARFIMAX model; Banach's Fixed-Point Theorem; numerical integral equation method; explicit method

I. INTRODUCTION

Control charts are fundamental tools in statistical process control. They are widely used to evaluate process stability and detect special-cause variations [1]. Their primary objective is to quickly identify deviations so that corrective measures can be applied, restoring the process to its in-control state. In detecting large parameter shifts, the Shewhart control chart is an effective tool; however, it is less efficient for small to moderate shifts. To address this limitation, more sensitive charts, such as CUSUM [2] and Exponentially Weighted Moving Average (EWMA) [3], have been developed. The upper-sided CUSUM chart is particularly useful when monitoring positive process increments, such as temperature or cost, in applications like semiconductor manufacturing and medical diagnostics [4, 5]. Building on these advantages, the present study proposes the upper-sided CUSUM control chart to enhance the detection of mean changes.

The performance of control charts is typically measured using ARL [6], defined as the expected number of samples until an out-of-control signal occurs. This metric is crucial for evaluating how efficiently and responsively a chart can detect process changes [7-9]. Several studies have examined ARL estimation for processes exhibiting normality or autocorrelation. Authors in [10] employed Markov chain and numerical IE methods to approximate the ARL of CUSUM and EWMA charts. In [11], ARL solutions were proposed for CUSUM charts with serial correlation, while authors in [12, 13] derived analytical and numerical ARL solutions for long-memory ARFIMA processes under EWMA monitoring. Motivated by these studies, the current research investigates an explicit ARL method based on the IE approach to improve CUSUM performance in detecting mean shifts.

In addition to the ARL, other metrics, such as the Median Run Length (MDRL) and the Standard Deviation of the Run Length (SDRL), are also valuable [1, 14]. The MDRL provides insight into the central tendency of the run length distribution, particularly when skewness is present, while the SDRL reflects its variability. Careful evaluation and comparison of these measures are necessary to fully assess the monitoring capability of the control charts. Thus, these indicators are incorporated to validate the proposed method.

Research on ARL performance has increasingly focused on autocorrelated or long-memory processes [15-17]. The Autoregressive Fractionally Integrated Moving Average with Exogenous Variables (ARFIMAX) model of order (p, d, q, x)(P, D, Q)$_L$ extends the classical ARFIMA model [18]. By integrating fractional differencing, seasonal effects, and external covariates, ARFIMAX captures complex temporal structures in data, such as environmental monitoring, industrial operations, and financial markets. In particular, when combined with exponentially distributed white noise, the ARFIMAX(p, d, q, x)(P, D, Q)$_L$ model under a CUSUM chart provides a robust framework for monitoring real-world systems [19]. This forms the central focus of the present study.

Although existing ARL approximation methods for such scenarios [20-22] provide accurate results, they are computationally expensive, so this study proposes an explicit ARL derivation method based on the IE approach for the ARFIMAX(p, d, q, x)(P, D, Q)$_L$ model with exponential white noise. The proposed method significantly reduces the computation time while maintaining high accuracy. Moreover, the performance of the CUSUM control chart under this method is compared with existing approximation techniques. Additional evaluation metrics, including the MDRL, SDRL, percentage accuracy (%Acc), and percentage relative deviation (%Dev), are employed for detailed analysis. Finally, the method is validated through a real-life application, confirming its practical value.

II. THE UPPER-SIDED CUSUM CONTROL CHART AND THE TIME SERIES MODEL

A. The Upper-Sided CUSUM Control Chart

The CUSUM statistic at time t, for detecting an upward shift from the in-control to the out-of-control state with observation Y_t can be computed by:

$$C_t = \max\left\{0,\, C_{t-1} + Y_t - K\right\} \quad (1)$$

for t=1,2,… and $C_0 = \upsilon$, when $\upsilon \le H$

where H represents the upper control limit, the reference value K is usually chosen as the ideal for detection, Y_t is a generalization of the ARFIMAX(p, d, q, x)(P, D, Q)$_L$ process with exogenous variables and underlying exponential white noise.

Monitoring the changes in the mean of a process on the CUSUM control chart involves determining the stopping time, which is the first instance when the mean exceeds a specified threshold. This threshold is employed as a decision boundary to indicate a statistically significant deviation from the target mean. The stopping time τ_H is defined by:

$$\tau_H = \inf\left\{ t > 0 : C_t > H \right\} \quad (2)$$

B. The ARFIMAX(p, d, q, x)(P, D, Q)$_L$ Model

The ARFIMAX(p, d, q, x)(P, D, Q)$_L$ model is a flexible time series framework that incorporates long memory, seasonal behavior, and external predictors. It consists of both non-seasonal and seasonal components.

In non-seasonal components, p represents the order of the Autoregressive (AR) term, d is the degree of fractional differencing (capturing long memory), q denotes the Moving Average (MA) order, and x is the number of exogenous variables.

In seasonal components, P is the order of seasonal AR, D is the degree of seasonal differencing, Q is the seasonal MA order, and L denotes the seasonal period, which means L=12 for monthly data with annual seasonality [15, 16].

The model can be expressed by:

$$\left.\begin{aligned} &\phi(B)\Phi(B^L)(1-B)^d(1-B^L)^D Y_t = \\ &= \sum_{h=1}^{n}\left(\omega_h X_{ht}\right) + \theta(B)\Theta(B^L)\varepsilon_t \end{aligned}\right\} \quad (3)$$

where X_{ht} are exogenous variables, ω_h are unknown parameters, ε_t is the exponentially distributed white noise with $\varepsilon_t \sim Exp(\lambda)$, and ϕ, θ, Φ, and Θ are polynomials with orders $p, q, P,$ and Q, respectively, which are defined as:

$$\left.\begin{aligned} &\phi_p(B) = 1 - \sum_{i=1}^{p}\phi_i B^i,\ \theta_q(B) = 1 - \sum_{j=1}^{q}\theta_j B^j, \\ &\Phi_P(B^L) = 1 - \sum_{k=1}^{P}\Phi_k B^{kL}, \Theta_Q(B^L) = 1 - \sum_{l=1}^{Q}\Theta_l B^{lL} \end{aligned}\right\} \quad (4)$$

where φ and θ are non-seasonal parameters, Φ and Θ are seasonal parameters, B is the backward shift operator, and $BY_t = Y_{t-1}$, $B^L Y_t = Y_{t-L}$ and $(1-B)^d, (1-B^L)^D$ are the non-seasonal and seasonal fractional differencing operators, respectively, both allowing for long-memory or persistent autocorrelation processes with non-integer values of d and D in the range [-0.5, 0.5] for $|d + D| < 0.5$.

The fractional differencing operator can be expanded using the binomial series:

$$(1-B^\ell)^\partial = \sum_{v=0}^{\infty}\binom{\partial}{v}(-B^\ell)^v \quad (5)$$

where $\binom{\partial}{v}$ is defined by:

$$\binom{\partial}{v} = \frac{\Gamma(\partial+1)}{\Gamma(v+1)\Gamma(\partial-v+1)} \quad (6)$$

where Γ denotes the gamma function.

Rearranging (3) and (5) gives:

$$\left.\begin{aligned} Y_t &= \sum_{h=1}^{n}\left(\omega_h X_{ht}\right) + \\ &+\frac{(1-\sum_{j=1}^{q}\theta_j B^j)(1-\sum_{l=1}^{Q}\Theta_l B^{lL})\varepsilon_t}{(1-\sum_{i=1}^{p}\phi_i B^i)(1-\sum_{k=1}^{P}\Phi_k B^{kL})(1-B)^d(1-B^L)^D} \end{aligned}\right\} \quad (7)$$

The inverse forms of the fractional differencing operators are given by $(1-B)^{-d}$ and $(1-B^L)^{-D}$.

Accordingly, the generalized ARFIMAX(*p, d, q, x*)(*P, D, Q*)$_L$ process with exogenous variables and exponentially distributed white noise, under CUSUM monitoring, can be expressed by:

$$\left.\begin{aligned} Y_t &= \sum_{h=1}^{n}\left(\omega_h X_{ht}\right) + (1-\sum_{i=1}^{p}\phi_i B^i)^{-1}(1-\sum_{k=1}^{P}\Phi_k B^{kL})^{-1}\cdot \\ &\cdot(1-B)^{-d}(1-B^L)^{-D}(1-\sum_{j=1}^{q}\theta_j B^j)(1-\sum_{l=1}^{Q}\Theta_l B^{lL})\varepsilon_t \end{aligned}\right\} \quad (8)$$

III. METHODOLOGY

A. The Proposed Method

Let $\mathcal{L}_p(\upsilon)$ be the ARL of the upper-sided CUSUM control chart based on the initial value υ of the process being monitored: an ARFIMAX(*p, d, q, x*)(*P, D, Q*)$_L$ model with exponential white noise. The ARL can be explicitly defined as:

$$\mathcal{L}_p(\upsilon) = \mathbb{E}_c(\tau_H) < \infty \quad (9)$$

where $\mathbb{E}_c$ is the mathematical expectation.

The IE for the ARL derived using the Fredholm IE of the second kind is expressed as:

$$\left.\begin{aligned} \mathcal{L}_p(\upsilon) &= 1 + \mathcal{L}_p(0)F\left(K-\upsilon-Y_t\right) + \\ &+\int_0^H \mathcal{L}_p(g)f(g+K-\upsilon-Y_t)dg \end{aligned}\right\} \quad (10)$$

where f and F are the probability density function (pdf) and cumulative distribution function (cdf) of an exponential distribution, respectively.

Hence, the IE for the ARL is defined by:

$$\begin{aligned} \mathcal{L}_p(\upsilon) = 1 &+ \mathcal{L}_p(0)\cdot\left(1-\exp\left\{-\lambda\left(K-\upsilon-\left(\begin{aligned}&\sum_{h=1}^{n}\left(\omega_h X_{ht}\right)+(1-\sum_{i=1}^{p}\phi_i B^i)^{-1}(1-\sum_{k=1}^{P}\Phi_k B^{kL})^{-1}(1-B)^{-d}(1-B^L)^{-D}\cdot \\ &\cdot(1-\sum_{j=1}^{q}\theta_j B^j)(1-\sum_{l=1}^{Q}\Theta_l B^{lL})\varepsilon_t\end{aligned}\right)\right)\right\}\right) + \\ &+\lambda\exp\left\{\lambda\left(-K+\upsilon+\left(\sum_{h=1}^{n}\left(\omega_h X_{ht}\right)+(1-\sum_{i=1}^{p}\phi_i B^i)^{-1}(1-\sum_{k=1}^{P}\Phi_k B^{kL})^{-1}(1-B)^{-d}(1-B^L)^{-D}(1-\sum_{j=1}^{q}\theta_j B^j)(1-\sum_{l=1}^{Q}\Theta_l B^{lL})\varepsilon_t\right)\right)\right\}\cdot \\ &\cdot\int_0^H \mathcal{L}_p(g)\exp\{-\lambda g\}dg \end{aligned} \quad (11)$$

Subsequently, Banach's Fixed Point Theorem was employed to ensure the existence and uniqueness of the ARL solution [20] for long-memory ARFIMAX processes, guaranteeing iterative convergence. This establishes both the theoretical soundness of the model and its practical reliability for efficient ARL computation.

Banach's fixed point theorem (Contraction Mapping Theorem) [21]:

Let $(M,\mathcal{D})$ be a complete metric space and $T: M \to M$ be a contraction mapping on *M*, if exists $\rho \in [0,1)$ such that:

$$\mathcal{D}\left(T(\mathcal{L}_1), T(\mathcal{L}_0)\right) \le \rho\cdot\mathcal{D}\left(\mathcal{L}_1,\mathcal{L}_0\right), \text{ for all } \mathcal{L}_1,\mathcal{L}_0 \in M$$

where $\mathcal{D}\left(\mathcal{L}_1,\mathcal{L}_0\right)$ represents the distance between $\mathcal{L}_1$ and $\mathcal{L}_0$ in metric space *M*, and ρ is the contraction constant. Subsequently:

1. There exists a unique fixed point $\mathcal{L}^* \in M$ such that: $T(\mathcal{L}^*) = \mathcal{L}^*$.
2. For any arbitrary element $\mathcal{L}_0 \in M$, the sequence is defined by:

$$\mathcal{L}_n = T(\mathcal{L}_{n-1}),\ n = 1,2,... \quad (12)$$

converges to a unique fixed point $\mathcal{L}^*$, and the convergence is geometric, characterized by the bound:

$$\mathcal{D}\left(\mathcal{L}^*, \mathcal{L}_n\right) \le \frac{\rho^n}{1-\rho} d\left(\mathcal{L}_1, \mathcal{L}_0\right).$$

Proof of existence: Let T be a contraction in a complete metric space $(M,\mathcal{D})$ and $C(I)$ represent the space of all continuous functions of $\mathcal{L}(\upsilon)$ on the interval $I = [0,H]$, where $\mathcal{L} \in M$. Defining a sequence of iterations $\{\mathcal{L}_n\}_{n\in\mathbf{N}}$ in M by setting $\mathcal{L}_n = T(\mathcal{L}_{n-1})$ for all $n \in \mathbf{N}$ yields the inequality:

$$\mathcal{D}\left(\mathcal{L}_{n+1},\mathcal{L}_n\right) \le \rho^n \mathcal{D}\left(\mathcal{L}_1,\mathcal{L}_0\right) \quad (13)$$

Given $m,n \in \mathbf{N}$ for $m > n$, then:

$$\mathcal{D}\left(\mathcal{L}_m,\mathcal{L}_n\right) \le \mathcal{D}\left(\mathcal{L}_m,\mathcal{L}_{m-1}\right)+\mathcal{D}\left(\mathcal{L}_{m-1},\mathcal{L}_{m-2}\right)+\ldots+\mathcal{D}\left(\mathcal{L}_{n+1},\mathcal{L}_n\right) \le$$
$$\le \rho^n \mathcal{D}\left(\mathcal{L}_1,\mathcal{L}_0\right)\sum_{i=0}^{\infty}\rho^i = \frac{\rho^n}{1-\rho}\mathcal{D}\left(\mathcal{L}_1,\mathcal{L}_0\right),$$

which leads to the conclusion that $\left\{\mathcal{L}_n\right\}_{n\in\mathbf{N}}$ is a Cauchy sequence. Since $(M,\mathcal{D})$ is a complete metric space, every Cauchy sequence has a limit point in *M*. So $\lim_{n\to\infty} T^n\left(\mathcal{L}_n\right) \to \mathcal{L}^*$ with $\mathcal{L}^* \in M$, which means $T(\mathcal{L}^*) = \mathcal{L}^*$.

Proof of uniqueness:

Suppose there are two fixed points $\mathcal{L}^*$ and K^* such that $T(\mathcal{L}^*) = \mathcal{L}^*$ and $T(K^*) = K^*$. Then:

$$\mathcal{D}\left(\mathcal{L}^*,K^*\right) = \mathcal{D}\left(\mathrm{T}\mathcal{L}^*,\mathrm{T}K^*\right) \le \rho\mathcal{D}\left(\mathcal{L}^*,K^*\right)$$

Since $\rho \in [0,1)$ the only solution is $\mathcal{D}\left(\mathcal{L}^*,K^*\right)=0$, implying that $\mathcal{L}^* = K^*$. Thus, the fixed point is unique.

Having established the existence and uniqueness of the IE solution, the explicit method can be derived for analyzing the ARL of the upper-sided CUSUM control chart applied to the ARFIMAX model with exponential white noise.

By substituting $s = \int_0^H \mathcal{L}_p(g)\exp\{-\lambda g\}dg$ in (11) and setting $\upsilon = 0$, (14) is obtained:

$$\mathcal{L}_p(0) = 1+\mathcal{L}_p(0)\cdot$$
$$\cdot\left(1-\exp\left\{-\lambda\left(K-\left(\begin{array}{l}\sum_{h=1}^{n}\left(\omega_h X_{ht}\right)+(1-\sum_{i=1}^{p}\phi_i B^i)^{-1}\cdot\\ \cdot(1-\sum_{k=1}^{P}\Phi_k B^{kL})^{-1}(1-B)^{-d}\cdot\\ \cdot(1-B^L)^{-D}(1-\sum_{j=1}^{q}\theta_j B^j)\cdot\\ \cdot(1-\sum_{l=1}^{Q}\Theta_l B^{lL})\varepsilon_t\end{array}\right)\right)\right\}\right)$$
$$+s\lambda\exp\left\{\lambda\left(-K+\left(\begin{array}{l}\sum_{h=1}^{n}\left(\omega_h X_{ht}\right)+(1-\sum_{i=1}^{p}\phi_i B^i)^{-1}\cdot\\ \cdot(1-\sum_{k=1}^{P}\Phi_k B^{kL})^{-1}(1-B)^{-d}\cdot\\ \cdot(1-B^L)^{-D}(1-\sum_{j=1}^{q}\theta_j B^j)\cdot\\ \cdot(1-\sum_{l=1}^{Q}\Theta_l B^{lL})\varepsilon_t\end{array}\right)\right)\right\} \quad (14)$$

By substituting $\mathcal{L}(0)$ from (14) into (11), the following expression is obtained:

$$\mathcal{L}_p(\upsilon) = 1+s\lambda+$$
$$+\exp\left\{\lambda\left(K-\left(\begin{array}{l}\sum_{h=1}^{n}\left(\omega_h X_{ht}\right)+(1-\sum_{i=1}^{p}\phi_i B^i)^{-1}\cdot\\ \cdot(1-\sum_{k=1}^{P}\Phi_k B^{kL})^{-1}(1-B)^{-d}\cdot\\ \cdot(1-B^L)^{-D}(1-\sum_{j=1}^{q}\theta_j B^j)\cdot\\ \cdot(1-\sum_{l=1}^{Q}\Theta_l B^{lL})\varepsilon_t\end{array}\right)\right)\right\}- \quad (15)$$
$$-\exp\{\lambda\upsilon\}$$

Accordingly, constant *s* can be reformulated as:

$$s = \lambda^{-1}\exp\{\lambda H\}\cdot$$
$$\cdot\left(1+\exp\left\{\lambda\left(K-\left(\begin{array}{l}\sum_{h=1}^{n}\left(\omega_h X_{ht}\right)+(1-\sum_{i=1}^{p}\phi_i B^i)^{-1}\cdot\\ \cdot(1-\sum_{k=1}^{P}\Phi_k B^{kL})^{-1}(1-B)^{-d}\cdot\\ \cdot(1-B^L)^{-D}(1-\sum_{j=1}^{q}\theta_j B^j)\cdot\\ \cdot(1-\sum_{l=1}^{Q}\Theta_l B^{lL})\varepsilon_t\end{array}\right)\right)\right\}\right)\cdot \quad (16)$$
$$\cdot(1-\exp\{-\lambda H\})-H\exp\{-\lambda H\}$$

Finally, substituting *s* from (16) into (15) yields:

$$\mathcal{L}_p(\upsilon) = \exp\{\lambda H\}\cdot$$
$$\cdot\left(1+\exp\left\{\lambda\left(K-\left(\begin{array}{l}\sum_{h=1}^{n}\left(\omega_h X_{ht}\right)+(1-\sum_{i=1}^{p}\phi_i B^i)^{-1}\cdot\\ \cdot(1-\sum_{k=1}^{P}\Phi_k B^{kL})^{-1}(1-B)^{-d}\cdot\\ \cdot(1-B^L)^{-D}(1-\sum_{j=1}^{q}\theta_j B^j)\cdot\\ \cdot(1-\sum_{l=1}^{Q}\Theta_l B^{lL})\varepsilon_t\end{array}\right)\right)\right\}\right)- \quad (17)$$
$$-\lambda H\big)-\exp\{\lambda\upsilon\}, \text{ with } \upsilon \ge 0.$$

Based on (17), the in-control ARL (ARL_0) is assumed to follow an exponential parameter ($\lambda = \lambda_0$), and the out-of-control ARL (ARL_1) is also assumed to follow an exponential parameter ($\lambda = \lambda_1$).

B. The NIE Benchmark Methods

The NIE method is using three rules: Midpoint, Trapezoidal, and Simpson's [19] to calculate approximated ARL derivations.

Equation (11) can be solved using finite approximation through the area rule $\{\ell_k, k=1,2,...,m\}$ on the interval $[0,H]$ and then apply the weighted constant $\{w_k, k=1,2,...,m\}$ as:

$$\int_0^H W(g)f(g)dg \approx \sum_{k=1}^{m} w_k f(\ell_k) \tag{18}$$

where $W(g)$ is a weight function, $f(g)$ is a function to be integrated on finite interval $[0,H]$, and ℓ_k is a set of points.

1) The Midpoint Rule

The approximation of the ARL $\hat{\mathcal{L}}_M(\upsilon)$, utilizing the Midpoint Rule based on the IE in (11), becomes:

$$\begin{aligned}
&\hat{\mathcal{L}}_M(\upsilon) \approx \\
&\approx 1+ \hat{\mathcal{L}}_M(\ell_1)F(K-\upsilon) - \left(\sum_{h=1}^{n}(\omega_h X_{ht}) + (1-\sum_{i=1}^{p}\phi_i B^i)^{-1} \cdot \right. \\
&\cdot(1-\sum_{k=1}^{P}\Phi_k B^{kL})^{-1}(1-B)^{-d}(1-B^L)^{-D}(1-\sum_{j=1}^{q}\theta_j B^j)\cdot \\
&\left. \cdot(1-\sum_{l=1}^{Q}\Theta_l B^{lL})\varepsilon_t \right) + \sum_{k=1}^{m} w_k \hat{\mathcal{L}}_M(\ell_k) f(\ell_k + K - \ell_j) - \\
&- \left(\sum_{h=1}^{n}(\omega_h X_{ht}) + (1-\sum_{i=1}^{p}\phi_i B^i)^{-1}(1-\sum_{k=1}^{P}\Phi_k B^{kL})^{-1} \cdot \right. \\
&\left. \cdot(1-B)^{-d}(1-B^L)^{-D}(1-\sum_{j=1}^{q}\theta_j B^j)(1-\sum_{l=1}^{Q}\Theta_l B^{lL})\varepsilon_t \right)
\end{aligned} \tag{19}$$

where $w_j = H/m$ and $\ell_k = (k-1/2)w_k$ for $k=1,2,...,m$.

2) The Trapezoidal Rule

Using the Trapezoidal Rule arises:

$$\begin{aligned}
&\hat{\mathcal{L}}_T(\upsilon) \approx \\
&\approx 1+ \hat{\mathcal{L}}_T(\ell_1)F(K-\upsilon) - \left(\sum_{h=1}^{n}(\omega_h X_{ht}) + (1-\sum_{i=1}^{p}\phi_i B^i)^{-1} \cdot \right. \\
&\cdot(1-\sum_{k=1}^{P}\Phi_k B^{kL})^{-1}(1-B)^{-d}(1-B^L)^{-D}(1-\sum_{j=1}^{q}\theta_j B^j)\cdot \\
&\left. \cdot(1-\sum_{l=1}^{Q}\Theta_l B^{lL})\varepsilon_t \right) + \sum_{k=1}^{m+1} w_k \hat{\mathcal{L}}_M(\ell_k) f(\ell_k + K - \ell_j) - \\
&- \left(\sum_{h=1}^{n}(\omega_h X_{ht}) + (1-\sum_{i=1}^{p}\phi_i B^i)^{-1}(1-\sum_{k=1}^{P}\Phi_k B^{kL})^{-1} \cdot \right. \\
&\left. \cdot(1-B)^{-d}(1-B^L)^{-D}(1-\sum_{j=1}^{q}\theta_j B^j)(1-\sum_{l=1}^{Q}\Theta_l B^{lL})\varepsilon_t \right)
\end{aligned} \tag{20}$$

where $w_k = H/m$ and $\ell_k = kw_k$ for $k=1,2,...,m-1$.

3) Simpson's Rule

Using Simpson's Rule, $\hat{\mathcal{L}}_M(\upsilon)$ becomes:

$$\begin{aligned}
&\hat{\mathcal{L}}_S(\upsilon) \approx \\
&\approx 1+ \hat{\mathcal{L}}_S(\ell_1)F(K-\upsilon) - \left(\sum_{h=1}^{n}(\omega_h X_{ht}) + (1-\sum_{i=1}^{p}\phi_i B^i)^{-1} \cdot \right. \\
&\cdot(1-\sum_{k=1}^{P}\Phi_k B^{kL})^{-1}(1-B)^{-d}(1-B^L)^{-D}(1-\sum_{j=1}^{q}\theta_j B^j)\cdot \\
&\left. \cdot(1-\sum_{l=1}^{Q}\Theta_l B^{lL})\varepsilon_t \right) + \sum_{k=1}^{2m+1} w_k \hat{\mathcal{L}}_S(\ell_k) f(\ell_k + K - \ell_j) - \\
&- \left(\sum_{h=1}^{n}(\omega_h X_{ht}) + (1-\sum_{i=1}^{p}\phi_i B^i)^{-1}(1-\sum_{k=1}^{P}\Phi_k B^{kL})^{-1} \cdot \right. \\
&\left. \cdot(1-B)^{-d}(1-B^L)^{-D}(1-\sum_{j=1}^{q}\theta_j B^j)(1-\sum_{l=1}^{Q}\Theta_l B^{lL})\varepsilon_t \right)
\end{aligned} \tag{21}$$

where $\ell_k = kw_k$ and

$$w_k = \begin{cases} 4/3(H/2m) \text{ when } k = 1,3,...,2m-1 \\ w_k = 2/3(H/2m) \text{ when } k = 2,4,...,2m-2 \end{cases}$$

C. RL Characteristics

To assess the in-control performance of the CUSUM control chart, predefined ARL_0 values of 370 and 500 were employed. These values correspond to Type I error rates of 0.0027 and 0.002, respectively. Conversely, the Type II error rate represents the probability of failing to detect a mean shift when the process is actually in the out-of-control state.

The performance of the control chart is typically evaluated using Run Length (RL)-based statistics, including ARL, MDRL, and SDRL:

- For the in-control state: $ARL_0 = 1/\lambda_0$, $MRL_0 = \log(0.5)/\log(1-\lambda_0)$, and $SDRL_0 = \sqrt{(1-\lambda_0)/\lambda_0^2}$
- For the out-f-control state: $ARL_1 = 1/\lambda_1$, $MRL_1 = \log(0.5)/\log(1-\lambda_1)$, and $SDRL_1 = \sqrt{(1-\lambda_1)/\lambda_1^2}$

A smaller SDRL indicates that the chart signals more consistently, whereas a larger SDRL suggests greater variability. Together, ARL, MDRL, and SDRL provide a comprehensive characterization of the control chart effectiveness.

IV. OVERALL PERFORMANCE METRICS

To comprehensively assess the proposed method, the following statistical and computational performance measures were employed.

A. Percentage Accuracy (%Acc)

The percentage accuracy is defined as:

$$\%\text{Acc} = 100 - \left| \frac{\mathcal{L}_P(\upsilon) - \mathcal{L}_N(\upsilon)}{\mathcal{L}_P(\upsilon)} \right| \times 100\% \quad (22)$$

where $\mathcal{L}_P(\upsilon)$ and $\mathcal{L}_N(\upsilon)$ represent the ARL values obtained using the proposed explicit method and the benchmark NIE method, respectively. A value of $\%\text{Acc} \approx 100\%$ reflects near-perfect agreement.

B. Percentage Relative Deviation (%Dev)

The percentage relative deviation is used to evaluate the responsiveness of the proposed method in detecting shifts of different magnitudes. It is given by:

$$\%\text{Dev} = \left| \frac{\mathcal{L}_{P1}(\upsilon) - \mathcal{L}_{P0}(\upsilon)}{\mathcal{L}_{P0}(\upsilon)} \right| \times 100\% \quad (23)$$

where $\mathcal{L}_{P0}(\upsilon)$ and $\mathcal{L}_{P1}(\upsilon)$ represent the ARLs computed using the proposed explicit method under the in-control and out-of-control states, respectively. The lowest %Dev value indicates the shift size that is detected most rapidly.

C. Computational Efficiency Analysis

In addition to statistical accuracy, computational efficiency was systematically assessed. The execution times required by the proposed explicit method and the benchmark NIE methods (Midpoint, Trapezoidal, and Simpson's Rules) were recorded under identical conditions. This enabled a direct comparison of the efficiency gains and highlighted the suitability of the proposed method for real-time monitoring applications, where rapid computation is essential.

V. NUMERICAL RESULTS

An algorithm was implemented in Mathematica to compute the ARL values using both the proposed explicit method and the benchmark NIE methods. The numerical results were generated with 500 division points for each process mean shift size δ, where $\delta \in \{0.75, 1.50, 2.25, 3.00, 3.75, 4.50\}$. The parameter values used in the optimal design of the upper-sided CUSUM chart are summarized in Table I.

The reference values (K) and corresponding control limits (H) for ARFIMAX models with long-memory and seasonal components ensure that the target ARL_0 (370 or 500) was achieved. The models differ in the order of their seasonal MA components (lag 12, order 1 or 2). The coefficient values for the non-seasonal and seasonal AR and MA terms were set to 0.1, while the second-order seasonal MA coefficient (Θ_2) was set to 0.2.

TABLE I. PARAMETER VALUES

ARFIMAX (p, d, q, x)(P, D, Q)$_L$	**ARL_0**	**K**		
		2.50	2.75	3.00
(1, 1/10, 1, 1)(1, 1/3, 1)12	370	4.8711219	4.2334253	3.8062265
	500	5.3565730	4.6035664	4.1474905
(1, 1/10, 1, 1)(1, 1/3, 2)12	370	4.0149468	3.6307145	3.2990654
	500	4.3680933	3.9642810	3.6220237

The simulation results for the out-of-control state (ARL_1) obtained using the proposed method and the various NIE approaches were evaluated across varying levels of mean shifts (Tables II, III) using the ARFIMAX(1, 1/10, 1, 1)(1, 1/3, 1)$_{12}$ and ARFIMAX(1, 1/10, 1,1)(1, 1/3, 2)$_{12}$ models, with both long-memory and seasonal components. All three NIE-based methods demonstrated strong performance in detecting small to moderate shifts in the process mean. Notably, the Simpson's Rule yielded slightly lower ARL_1 values compared to both the Midpoint and Trapezoidal Rules across all shift magnitudes.

TABLE II. COMPARISON OF ARL_1 VALUES FOR ARFIMAX(1, 1/10, 1, 1)(1, 1/3, 1)$_{12}$ MODEL

ARL_0	**K**	**δ**	**0.75**		**1.50**		**2.25**		**3.00**		**3.75**		**4.50**	
370	2.50	$\mathcal{L}_P(\upsilon)$	17.457	(a.)	6.896	(a.)	4.454	(a.)	3.423	(a.)	2.860	(a.)	2.507	(a.)
		$\hat{\mathcal{L}}_M(\upsilon)$	17.453	(7.735)	6.896	(7.714)	4.454	(7.660)	3.423	(7.731)	2.860	(7.707)	2.507	(7.685)
		$\hat{\mathcal{L}}_T(\upsilon)$	18.258	(8.498)	6.989	(8.501)	4.481	(8.571)	3.435	(8.612)	2.866	(8.558)	2.510	(8.566)
		$\hat{\mathcal{L}}_S(\upsilon)$	17.240	(72.357)	6.869	(71.843)	4.445	(72.027)	3.418	(71.811)	2.857	(72.171)	2.505	(72.481)
	2.75	$\mathcal{L}_P(\upsilon)$	20.807	(a.)	7.620	(a.)	4.669	(a.)	4.669	(a.)	2.870	(a.)	2.493	(a.)
		$\hat{\mathcal{L}}_M(\upsilon)$	20.784	(7.456)	7.617	(7.393)	4.668	(7.478)	3.487	(7.429)	2.869	(7.441)	2.493	(7.430)
		$\hat{\mathcal{L}}_T(\upsilon)$	21.229	(9.213)	7.674	(9.575)	4.685	(9.667)	3.495	(9.814)	2.874	(9.769)	2.496	(9.316)
		$\hat{\mathcal{L}}_S(\upsilon)$	20.550	(70.363)	7.590	(70.369)	4.659	(70.350)	3.483	(70.539)	2.867	(0.048)	2.492	(71.637)
	3.00	$\mathcal{L}_P(\upsilon)$	22.700	(a.)	8.114	(a.)	4.851	(a.)	3.568	(a.)	2.907	(a.)	2.510	(a.)
		$\hat{\mathcal{L}}_M(\upsilon)$	22.670	(7.451)	8.109	(7.553)	4.849	(7.495)	3.567	(7.621)	2.906	(7.443)	2.510	(7.531)
		$\hat{\mathcal{L}}_T(\upsilon)$	22.950	(12.078)	8.149	(12.106)	4.862	(12.072)	3.573	(10.177)	2.910	(9.746)	2.512	(9.900)
		$\hat{\mathcal{L}}_S(\upsilon)$	22.449	(75.145)	8.084	(74.765)	4.842	(74.390)	3.563	(75.068)	2.904	(74.365)	2.508	(75.802)
500	2.50	$\mathcal{L}_P(\upsilon)$	17.682	(a.)	7.039	(a.)	4.615	(a.)	3.567	(a.)	2.985	(a.)	2.615	(a.)
		$\hat{\mathcal{L}}_M(\upsilon)$	17.693	(7.729)	7.042	(7.750)	4.616	(7.745)	3.568	(7.548)	2.985	(7.524)	2.615	(7.566)
		$\hat{\mathcal{L}}_T(\upsilon)$	19.012	(8.542)	7.178	(8.535)	4.654	(8.631)	3.584	(8.668)	2.993	(8.782)	2.620	(9.019)
		$\hat{\mathcal{L}}_S(\upsilon)$	17.449	(76.592)	7.011	(73.559)	4.605	(75.940)	3.562	(75.968)	2.982	(77.695)	2.613	(77.580)
	2.75	$\mathcal{L}_P(\upsilon)$	23.189	(a.)	8.141	(a.)	4.927	(a.)	3.658	(a.)	2.997	(a.)	2.595	(a.)

		$\hat{\mathcal{L}}_M(\upsilon)$	23.165	(7.572)	8.138	(7.506)	4.926	(7.478)	3.658	(7.504)	2.997	(7.502)	2.595	(7.531)
		$\hat{\mathcal{L}}_T(\upsilon)$	23.879	(9.098)	8.219	(9.059)	4.949	(9.106)	3.668	(9.077)	3.002	(9.116)	2.598	(9.074)
		$\hat{\mathcal{L}}_S(\upsilon)$	22.845	(69.678)	8.104	(71.728)	4.915	(71.544)	3.653	(71.745)	2.994	(71.289)	2.593	(70.723)
	3.00	$\mathcal{L}_P(\upsilon)$	25.883	(a.)	8.802	(a.)	5.163	(a.)	3.759	(a.)	3.043	(a.)	2.616	(a.)
		$\hat{\mathcal{L}}_M(\upsilon)$	25.847	(7.483)	8.796	(7.471)	5.161	(7.454)	3.758	(7.412)	3.043	(7.385)	2.615	(7.330)
		$\hat{\mathcal{L}}_T(\upsilon)$	26.294	(9.358)	8.854	(9.267)	5.178	(9.366)	3.766	(9.317)	3.047	(9.341)	2.618	(9.286)
		$\hat{\mathcal{L}}_S(\upsilon)$	25.530	(75.424)	8.764	(73.939)	5.151	(71.093)	3.754	(71.545)	3.040	(71.015)	2.614	(71.309)
The values in parentheses are the computation time in min.														

TABLE III. COMPARISON OF ARL_1 VALUES FOR ARFIMAX(1, 1/10, 1, 1)(1, 1/3, 2)$_{12}$ MODEL

ARL_0	**K**	**δ**	**0.75**		**1.50**		**2.25**		**3.00**		**3.75**		**4.50**	
370	2.50	$\mathcal{L}_P(\upsilon)$	21.809	(a.)	7.874	(a.)	4.759	(a.)	3.526	(a.)	2.886	(a.)	2.500	(a.)
		$\hat{\mathcal{L}}_M(\upsilon)$	21.782	(7.583)	7.869	(10.131)	4.758	(7.530)	3.525	(7.519)	2.886	(7.526)	2.499	(7.515)
		$\hat{\mathcal{L}}_T(\upsilon)$	22.134	(8.726)	7.917	(8.750)	4.773	(8.714)	3.532	(8.783)	2.889	(8.731)	2.502	(8.852)
		$\hat{\mathcal{L}}_S(\upsilon)$	21.551	(67.365)	7.843	(67.353)	4.750	(67.589)	3.521	(67.524)	2.884	(67.237)	2.498	(68.093)
	2.75	$\mathcal{L}_P(\upsilon)$	23.399	(a.)	8.313	(a.)	4.931	(a.)	3.606	(a.)	2.927	(a.)	2.521	(a.)
		$\hat{\mathcal{L}}_M(\upsilon)$	23.366	(7.570)	8.307	(7.607)	4.929	(7.597)	3.605	(7.549)	2.927	(7.564)	2.521	(7.569)
		$\hat{\mathcal{L}}_T(\upsilon)$	23.596	(8.769)	8.342	(8.743)	4.940	(8.734)	3.610	(8.728)	2.929	(8.869)	2.523	(8.758)
		$\hat{\mathcal{L}}_S(\upsilon)$	23.157	(66.321)	8.283	(66.522)	4.921	(67.538)	3.602	(67.516)	2.925	(67.269)	2.520	(67.286)
	3.00	$\mathcal{L}_P(\upsilon)$	24.587	(a.)	8.673	(a.)	5.082	(a.)	3.683	(a.)	2.971	(a.)	2.548	(a.)
		$\hat{\mathcal{L}}_M(\upsilon)$	24.553	(7.561)	8.666	(7.552)	5.080	(7.528)	3.681	(7.538)	2.970	(7.571)	2.547	(7.510)
		$\hat{\mathcal{L}}_T(\upsilon)$	24.709	(8.781)	8.692	(8.791)	5.089	(8.823)	3.686	(8.801)	2.972	(8.820)	2.549	(8.743)
		$\hat{\mathcal{L}}_S(\upsilon)$	24.371	(67.479)	8.645	(67.654)	5.073	(67.744)	3.679	(67.327)	2.968	(67.589)	2.546	(67.342)
500	2.50	$\mathcal{L}_P(\upsilon)$	24.633	(a.)	8.484	(a.)	5.045	(a.)	3.707	(a.)	3.018	(a.)	2.603	(a.)
		$\hat{\mathcal{L}}_M(\upsilon)$	24.601	(7.540)	8.479	(7.568)	5.044	(7.524)	3.706	(7.565)	3.017	(7.525)	2.603	(7.547)
		$\hat{\mathcal{L}}_T(\upsilon)$	25.166	(8.755)	8.548	(8.768)	5.064	(8.717)	3.715	(8.760)	3.022	(8.774)	2.606	(8.807)
		$\hat{\mathcal{L}}_S(\upsilon)$	24.279	(67.142)	8.446	(67.105)	5.034	(67.138)	3.701	(67.450)	3.015	(66.787)	2.601	(66.487)
	2.75	$\mathcal{L}_P(\upsilon)$	26.847	(a.)	9.061	(a.)	5.263	(a.)	3.806	(a.)	3.068	(a.)	2.629	(a.)
		$\hat{\mathcal{L}}_M(\upsilon)$	26.808	(7.580)	9.055	(7.542)	5.261	(7.570)	3.805	(7.573)	3.067	(7.565)	2.629	(7.547)
		$\hat{\mathcal{L}}_T(\upsilon)$	27.173	(8.737)	9.104	(8.843)	5.276	(0.088)	3.812	(8.824)	3.071	(0.051)	2.631	(8.769)
		$\hat{\mathcal{L}}_S(\upsilon)$	26.503	(67.744)	9.023	(67.476)	5.252	(67.415)	3.801	(67.421)	3.065	(67.702)	2.628	(67.866)
	3.00	$\mathcal{L}_P(\upsilon)$	28.467	(a.)	9.524	(a.)	5.452	(a.)	3.901	(a.)	3.121	(a.)	2.661	(a.)
		$\hat{\mathcal{L}}_M(\upsilon)$	28.424	(7.541)	9.516	(7.684)	5.450	(7.525)	3.899	(7.641)	3.120	(10.052)	2.660	(10.044)
		$\hat{\mathcal{L}}_T(\upsilon)$	28.671	(8.771)	9.554	(8.736)	5.462	(8.822)	3.905	(8.720)	3.123	(8.892)	2.662	(8.779)
		$\hat{\mathcal{L}}_S(\upsilon)$	28.152	(67.260)	9.488	(67.887)	5.441	(67.375)	3.896	(67.557)	3.118	(67.530)	2.659	(67.705)
The values in parentheses are the computation time in min.														

The computation times revealed notable differences in efficiency. Simpson's Rule required approximately 65–79 min, whereas the Midpoint and Trapezoidal rules needed 7–10 min. This substantial difference highlights the superior processing efficiency of the Midpoint and Trapezoidal approaches, making them more suitable for real-time or time-sensitive applications. In conclusion, selecting an appropriate NIE method requires balancing its accuracy and computational efficiency. Based on the simulation results, the Midpoint Rule was chosen as being the most suitable for verifying the accuracy of the proposed method.

Both the proposed and Midpoint Rule NIE methods produced similar ARL_1 values. Moreover, as the magnitude of the process mean shift increased, the corresponding ARL1 values consistently decreased, hence indicating enhanced detection sensitivity. The (%Acc) values are consistently close to 100% (Table IV), demonstrating excellent agreement between the proposed method and the Midpoint Rule NIE approach.

The reference value (K) for the CUSUM chart significantly influences its sensitivity in detecting process shifts. The results indicate that the proposed method exhibited the highest sensitivity for K = 2.50, followed by K = 2.75 and K = 3.00 for any combination of conditions. A shift size of 0.75 resulted in a %Dev of 95.2820% for K = 2.50 for the ARFIMAX(1, 1/10, 1, 1)(1, 1/3, 1)12 model with ARL_0 set to 370. In other cases, as the shift magnitude was increased, the %Dev also increased (Table IV). This suggests that the shift size with the lowest

%Dev was detected the most rapidly, which aligns with the results in [22]. Moreover, the MDRL and SDRL values (Table V) are consistent with the ARL results obtained using the proposed method. The results indicate that the MDRL and SDRL values exhibited the highest sensitivity for K = 2.50, followed by K = 2.75 and K = 3.00 for any combination of conditions.

TABLE IV. OVERALL PERFORMANCE METRICS COMPARING PROPOSED AND MIDPOINT RULE METHODS

ARL_0	K	Models	ARFIMAX(1, 1/10, 1, 1)(1, 1/3, 1)$_{12}$						ARFIMAX(1, 1/10, 1, 1)(1, 1/3, 2)$_{12}$					
		δ	0.75	1.50	2.25	3.00	3.75	4.50	0.75	1.50	2.25	3.00	3.75	4.50
370	2.50	%Acc	100.000	100.000	100.000	100.000	100.000	100.000	99.874	99.941	99.966	99.977	99.984	99.988
		%Dev	95.282	98.136	98.796	99.075	99.227	99.323	94.113	97.873	98.714	99.047	99.220	99.325
	2.75	%Acc	99.999	100.000	100.000	99.747	100.000	100.000	99.863	99.929	99.958	99.971	99.980	99.985
		%Dev	94.376	97.940	98.738	98.738	99.224	99.326	93.685	97.755	98.668	99.026	99.209	99.319
	3.00	%Acc	99.999	99.999	100.000	100.000	100.000	100.000	99.862	99.925	99.954	99.969	99.977	99.983
		%Dev	93.865	97.807	98.689	99.036	99.214	99.322	93.364	97.658	98.627	99.005	99.197	99.312
500	2.50	%Acc	99.999	100.000	100.000	100.000	100.000	100.000	99.873	99.943	99.968	99.979	99.984	99.988
		%Dev	96.464	98.592	99.077	99.287	99.403	99.477	93.351	97.708	98.637	98.998	99.185	99.297
	2.75	%Acc	99.999	100.000	100.000	100.000	100.000	100.000	99.854	99.927	99.957	99.971	99.980	99.984
		%Dev	95.362	98.372	99.015	99.268	99.401	99.481	92.755	97.553	98.578	98.972	99.171	99.290
	3.00	%Acc	99.999	99.999	100.000	100.000	100.000	100.000	99.850	99.920	99.951	99.967	99.976	99.982
		%Dev	94.823	98.240	98.968	99.248	99.391	99.477	92.318	97.428	98.527	98.946	99.157	99.281

TABLE V. COMPARISON OF RL CHARACTERISTICS OF PROPOSED METHOD FOR THE UPPER-SIDED CUSUM CHART

ARL_0	K	Models	ARFIMAX(1, 1/10, 1, 1)(1, 1/3, 1)$_{12}$						ARFIMAX(1, 1/10, 1, 1)(1, 1/3, 2)$_{12}$					
		δ	0.75	1.50	2.25	3.00	3.75	4.50	0.75	1.50	2.25	3.00	3.75	4.50
370	2.50	ARL	17.457	6.896	4.454	3.423	2.860	2.507	21.809	7.874	4.759	3.526	2.886	2.500
		SDRL	16.950	6.376	3.922	2.880	2.306	1.944	21.303	7.357	4.230	2.984	2.333	1.936
		MRL	0.242	0.359	0.464	0.563	0.660	0.754	0.225	0.336	0.444	0.550	0.654	0.756
	2.75	ARL	20.807	7.620	4.669	4.669	2.870	2.493	23.399	8.313	4.931	3.606	2.927	2.521
		SDRL	16.950	6.376	3.922	2.880	2.306	1.944	21.303	7.357	4.230	2.984	2.333	1.936
		MRL	0.242	0.359	0.464	0.563	0.660	0.754	0.225	0.336	0.444	0.550	0.654	0.756
	3.00	ARL	22.700	8.114	4.851	3.568	2.907	2.510	24.587	8.673	5.082	3.683	2.971	2.548
		SDRL	22.194	7.598	4.322	3.027	2.354	1.947	24.082	8.158	4.555	3.143	2.420	1.986
		MRL	0.222	0.331	0.439	0.545	0.650	0.753	0.216	0.321	0.426	0.532	0.637	0.741
500	2.50	ARL	17.682	7.039	4.615	3.567	2.985	2.615	24.633	8.484	5.045	3.707	3.018	2.603
		SDRL	17.175	6.520	4.085	3.026	2.434	2.055	24.128	7.968	4.517	3.168	2.468	2.043
		MRL	0.241	0.355	0.453	0.545	0.634	0.721	0.216	0.324	0.428	0.529	0.628	0.725
	2.75	ARL	23.189	8.141	4.927	3.658	2.997	2.595	26.847	9.061	5.263	3.806	3.068	2.629
		SDRL	22.683	7.625	4.399	3.118	2.446	2.034	26.342	8.546	4.737	3.268	2.519	2.069
		MRL	0.220	0.331	0.435	0.534	0.632	0.727	0.211	0.314	0.417	0.519	0.618	0.717
	3.00	ARL	25.883	8.802	5.163	3.759	3.043	2.616	28.467	9.524	5.452	3.901	3.121	2.661
		SDRL	25.378	8.287	4.636	3.220	2.493	2.056	27.963	9.010	4.927	3.364	2.573	2.102
		MRL	0.213	0.319	0.422	0.523	0.623	0.721	0.207	0.308	0.409	0.509	0.609	0.708

VI. REAL-LIFE APPLICABILITY

To demonstrate the practical utility of the proposed method, a case study is presented, examining the relationship between the oil and fuel export values and plant and animal oil exports as an exogenous variable, in the context of renewable energy. The dataset, obtained from the Bank of Thailand [23], comprises 37 monthly observations spanning January 2020 to December 2024, classified by product groups under exports and imports.

The ARFIMAX(p, d, q, x)(P, D, Q)$_L$ model was fitted, and parameter estimates were obtained using EViews 10, concluding that the one with the best overall fit is ARFIMAX(1, 0.4990, 1, 1)(1, 0.5858, 2)$_{12}$ (Table VI). Thus, the monthly export data were assumed to follow this specification, and the estimated parameters were applied in the process control analysis. A Kolmogorov–Smirnov (KS) test conducted with SPSS returned a probability value of 0.6677, confirming that the residuals follow an exponential distribution with parameter 2,057.31.

Based on the numerical results, the most effective configuration was the CUSUM control chart with settings of K = 2.50 and H = 2,509.983 or 3,133.709, corresponding to ARL_0 = 370 and 500, respectively. The ARL_1 values obtained using the proposed method (Table VII) showed close alignment with those of the NIE Midpoint Rule, with %Acc values being consistently near 100%.

TABLE VI. ESTIMATED PARAMETER VALUES

Model	Estimated parameters	Std. Error	t-Statistic	Prob.
ARFIMAX (p, d, q, x)(P, D, Q)$_L$	$\hat{\omega}_1$ =-0.9858	0.3297	-2.9897	0.0055
	$\hat{\phi}_1$ =-0.4937	0.0540	-9.1421	0.0000
	$\hat{d}$ =0.4990	0.0780	6.3978	0.0000
	$\hat{\theta}_1$ = 0.9152	0.1105	8.2792	0.0000

	$\hat{\Phi}_1$ = 1.0000	0.0011	904.1309	0.0000
	$\hat{D}$ = 0.5858	0.0612	9.5702	0.0000
	$\hat{\Theta}_1$ = -0.9851	0.1106	-8.9089	0.0000
Exponential white noise	KS test			0.7259
	Exponential parameter			2,057.3100
	Asymp. Sig. (2-tailed)			0.6677

Importantly, the proposed method required only a fraction of a second to compute, compared to several min for NIE-based methods. Furthermore, the proposed method identified the smallest %Dev for a shift size of 0.75, highlighting its sensitivity in detecting early deviations.

TABLE VII. COMPARISON OF ARL_1 VALUES FOR ARFIMAX(1, 0.4990, 1, 1)(1, 0.5858, 1)$_{12}$ MODEL

ARL_0	**K**	**Methods**	**δ**											
			0.75		**1.50**		**2.25**		**3.00**		**3.75**		**4.50**	
370	2.50	$\mathcal{L}_P(\upsilon)$	29.033	(a.)	10.502	(a.)	6.087	(a.)	4.334	(a.)	3.437	(a.)	2.904	(a.)
		$\hat{\mathcal{L}}_M(\upsilon)$	29.014	(7.565)	10.498	(7.471)	6.085	(7.628)	4.333	(7.515)	3.436	(7.472)	2.904	(7.457)
		$\hat{\mathcal{L}}_T(\upsilon)$	29.034	(8.834)	10.503	(8.743)	6.087	(8.829)	4.334	(8.961)	3.437	(8.874)	2.904	(8.890)
		$\hat{\mathcal{L}}_S(\upsilon)$	28.994	(67.153)	10.495	(67.296)	6.084	(67.389)	4.332	(67.025)	3.436	(67.652)	2.904	(67.789)
		%Acc	99.935		99.959		99.971		99.979		99.984		99.988	
		%Dev	92.153		97.162		98.355		98.829		99.071		99.215	
500	2.50	$\mathcal{L}_P(\upsilon)$	34.3	(a.)	11.762	(a.)	6.631	(a.)	4.643	(a.)	3.641	(a.)	3.053	(a.)
		$\hat{\mathcal{L}}_M(\upsilon)$	34.272	(7.425)	11.756	(7.476)	6.628	(7.458)	4.642	(7.489)	3.641	(7.600)	3.052	(7.555)
		$\hat{\mathcal{L}}_T(\upsilon)$	34.304	(11.852)	11.764	(11.701)	6.631	(12.290)	4.643	(12.535)	3.642	(11.715)	3.053	(11.279)
		$\hat{\mathcal{L}}_S(\upsilon)$	34.233	(68.247)	11.751	(67.739)	6.627	(67.615)	4.641	(66.909)	3.64	(71.630)	3.052	(72.431)
		%Acc	99.919		99.949		99.964		99.974		99.98		99.984	
		%Dev	93.14		97.648		98.674		99.071		99.272		99.389	
The values in parentheses are the computation time in min.														

For ARL_0 = 370, the first out-of-control signal was detected after the 3rd sample, with 10 total signals. For ARL_0 = 500, the first signal appeared after the 4th sample, with 6 signals in total (Figure 1). These results underscore the effectiveness of the proposed method in real-time detection using the CUSUM chart.

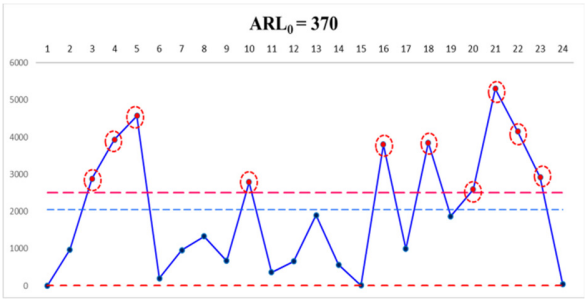

(a)

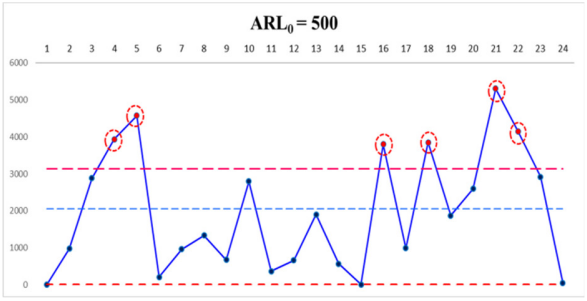

(b)

Fig. 1. ARFIMAX(1, 0.4990, 1, 1)(1, 0.5858, 1)$_{12}$: (a) ARL_0=370 with UCL=2,509.983, (b) ARL_0=500 with UCL=3,133.709.

VII. CONCLUSIONS

The present study introduced a novel explicit method for improving the detection of small-to-moderate mean shifts in long-memory ARFIMAX(p, d, q, x)(P, D, Q)$_L$ processes with exponential white noise using the upper-sided Cumulative Sum (CUSUM) chart. Among the design choices, K = 2.50 was found to provide the highest monitoring efficiency and can be proposed for applications targeting different in-control ARL values.

The proposed method outperformed benchmark NIE approaches in both percentage accuracy and computational efficiency and delivered fast ARL_1 computation for detecting small shifts (δ = 0.75) with minimal relative deviation. It also demonstrated a consistent RL behavior through the MDRL and SDRL metrics. Its effectiveness was further validated through a real-world case study, where the results aligned closely with simulation findings. Collectively, these outcomes highlight the method as a reliable and computationally superior alternative to traditional NIE-based ARL approximation techniques.

Future research can extend this work in several directions. First, the explicit method may be applied to other control charts, such as Exponentially Weighted Moving Average (EWMA), to compare the detection performance against the CUSUM chart. Second, it may be adapted for monitoring the changes in other process models relevant to practical applications. Finally, its extension to ARFIMAX processes with alternative white noise distributions within the exponential family warrants investigation.

ACKNOWLEDGMENT

The authors gratefully acknowledge the financial support provided by the National Science, Research and Innovation

Fund (NSRF) and King Mongkut's University of Technology North Bangkok (Contract No. KMUTNB-FF-68-B-45).

REFERENCES

[1] D. C. Montgomery, *Introduction to Statistical Quality Control*, 8th ed. Hoboken, NJ: Wiley, 2020.

[2] E. S. Page, "Continuous Inspection Schemes," *Biometrika*, vol. 41, no. 1–2, pp. 100–115, Jun. 1954, https://doi.org/10.1093/biomet/41.1-2.100.

[3] S. W. Roberts, "Control Chart Tests Based on Geometric Moving Averages," *Technometrics*, vol. 1, no. 3, pp. 239–250, Aug. 1959, https://doi.org/10.1080/00401706.1959.10489860.

[4] S. S. Cheng, F. J. Yu, and S. H. M. Wang, "A CUSUM Control Chart to Monitor Wafer Production Quality," *Journal of Information and Optimization Sciences*, vol. 35, no. 5–6, pp. 483–501, Nov. 2014, https://doi.org/10.1080/02522667.2014.943066.

[5] O. A. Grigg, V. T. Farewell, and D. J. Spiegelhalter, "Use of risk-adjusted CUSUM and RSPRTcharts for monitoring in medical contexts," *Statistical Methods in Medical Research*, vol. 12, no. 2, pp. 147–170, Apr. 2003, https://doi.org/10.1177/0962280203012002O5.

[6] M. Moameni, A. Saghaei, and M. G. Salanghooch, "The Effect of Measurement Error on $\tilde{X}$-$\tilde{R}$ Fuzzy Control Charts," *Engineering, Technology & Applied Science Research*, vol. 2, no. 1, pp. 173–176, Feb. 2012, https://doi.org/10.48084/etasr.127.

[7] C. W. Champ and S. E. Rigdon, "A comparison of the markov chain and the integral equation approaches for evaluating the run length distribution of quality control charts," *Communications in Statistics - Simulation and Computation*, vol. 20, no. 1, pp. 191–204, Apr. 1991, https://doi.org/10.1080/03610919108812948.

[8] E. Yashchin, "Performance of CUSUM Control Schemes for Serially Correlated Observations," *Technometrics*, vol. 35, no. 1, pp. 37–52, 1993, https://doi.org/10.1080/00401706.1993.10484992.

[9] R. Sunthornwat, Y. Areepong, and S. Sukparungsee, "Analytical and numerical solutions of average run length integral equations for an EWMA control chart over a long memory SARFIMA process," *Songklanakarin Journal of Science and Technology (SJST)*, vol. 40, no. 4, pp. 885–895, Aug. 2018, https://doi.org/10.14456/sjst-psu.2018.93.

[10] E. T. Herdiani, G. Fandrilla, and N. Sunusi, "Modified Exponential Weighted Moving Average (EWMA) Control Chart on Autocorrelation Data," *Journal of Physics: Conference Series*, vol. 979, no. 1, Nov. 2018, Art. no. 012097, https://doi.org/10.1088/1742-6596/979/1/012097.

[11] A. Fonseca *et al.*, "Water Particles Monitoring in the Atacama Desert: SPC Approach Based on Proportional Data," *Axioms*, vol. 10, no. 3, Sept. 2021, Art. no. 154, https://doi.org/10.3390/axioms10030154.

[12] D. R. Prajapati and S. Singh, "Control charts for monitoring the autocorrelated process parameters: a literature review," *International Journal of Productivity and Quality Management*, vol. 10, no. 2, pp. 207–249, Aug. 2012, https://doi.org/10.1504/IJPQM.2012.048298.

[13] J. A. Garza-Venegas, V. G. Tercero-Gómez, L. L. Ho, P. Castagliola, and G. Celano, "Effect of autocorrelation estimators on the performance of the $\bar{X}$ control chart," *Journal of Statistical Computation and Simulation*, vol. 88, no. 13, pp. 2612–2630, Sept. 2018, https://doi.org/10.1080/00949655.2018.1479752.

[14] A. A. Nadi, G. Celano, and S. Steiner, "Investigating the performance of the Phase II Hotelling T2 chart when monitoring multivariate time series observations." arXiv, Jan. 20, 2025, https://doi.org/10.48550/arXiv.2501.11649.

[15] H. Ebens, (1999). Realized Stock Volatility. Economics Working Paper Archive 420. Johns Hopkins University. Available at: https://ideas.repec.org/p/jhu/papers/420.html

[16] C. W. J. Granger and R. Joyeux, "An Introduction to Long-Memory Time Series Models and Fractional Differencing," *Journal of Time Series Analysis*, vol. 1, no. 1, pp. 15–29, 1980, https://doi.org/10.1111/j.1467-9892.1980.tb00297.x.

[17] J. R. M. Hosking, "Fractional differencing," *Biometrika*, vol. 68, no. 1, pp. 165–176, Apr. 1981, doi: 10.1093/biomet/68.1.165.

[18] P. Buranapol and S. Phanyaem, "Average Run Length of CUSUM Control Chart for SARX(P,1)L Model using Numerical Integral Equation Method," *Journal of Applied Science and Emerging Technology*, vol. 21, no. 1, June 2022, Art. no. 246470, https://doi.org/10.14416/j.appsci.2022.01.018.

[19] P. Paichit and W. Peerajit, "Development of a Numerical Approach to Evaluate the Performance of the CUSUM Control Chart for a Long Memory SARFIMA Model," *WSEAS Transactions on Systems and Control*, vol. 20, pp. 172–184, May 2025, https://doi.org/10.37394/23203.2025.20.20.

[20] B. V. Rao, R. L. Disney, and J. J. Pignatiello, "Uniqueness and convergence of solutions to average run length integral equations for cumulative sum and other control charts," *IIE Transactions*, vol. 33, no. 6, pp. 463–469, Jun. 2001, https://doi.org/10.1023/A:1007633828234.

[21] S. Banach, "On Operations in Abstract Sets and Their Application to Integral Equations," *Fundamenta Mathematicae*, vol. 3, no. 1, pp. 133–181, 1922.

[22] E. S. Page, "Cumulative Sum Charts," *Technometrics*, vol. 3, no. 1, pp. 1–9, Feb. 1961, https://doi.org/10.1080/00401706.1961.10489922.

[23] "Economic and Financial Index and Indicators," *Bank of Thailand*. https://www.bot.or.th/en/statistics/economic-and-financial-index-and-indicators.html.